AIP Journal of Applied Physics

Compositional depth profiles of chemiplated Cu2S/(Zn,Cd)S heterojunction solar cells

P. N. Uppal, L. C. Burton, L. Rivaud, and J. E. Greene

Citation: Journal of Applied Physics **54**, 982 (1983); doi: 10.1063/1.332024
View online: http://dx.doi.org/10.1063/1.332024
View Table of Contents: http://scitation.aip.org/content/aip/journal/jap/54/2?ver=pdfcov
Published by the AIP Publishing

Compositional depth profiles of chemiplated Cu_2S/(Zn,Cd)S heterojunction solar cells

P. N. Uppal, and L. C. Burton
Departments of Electrical and Materials Engineering, Virginia Polytechnic Institute and State University, Blacksburg, Virginia 24061

L. Rivaud and J. E. Greene
Department of Metallurgy, the Coordinated Science Laboratory and the Materials Research Laboratory, University of Illinois, Urbana, Illinois 61801

(Received 23 June 1982; accepted for publication 9 July 1982)

Atomic absorption spectroscopy combined with controlled chemical etching and Auger electron spectroscopy profiling with ion beam etching have been used to obtain composition versus depth analyses of Cu_2S/(Zn,Cd)S heterojunction solar cells formed by an aqueous cation exchange, or chemiplating, process. The Cu_2S films, ranging from 0.5 to 6 μm in thickness, were polycrystalline and exhibited a (001) preferred orientation on either textured polycrystalline or cleaved single crystal (Zn,Cd)S substrates. The profiling results showed that the interfacial regions were compositionally graded over very large distances ranging from tens to hundreds of nonometers depending on the Cu_2S film thickness. This is much wider than observed for comparable Cu_2S/CdS cells. Moreover, excess Zn in the form of both elemental Zn and ZnS was always found in the interfacial region and may be responsible for the short circuit current being lower than expected for these cells.

PACS numbers: 73.60.Dt, 72.15.Jf, 72.15.Eb, 81.15.Gh

I. INTRODUCTION

The Cu_2S/CdS thin film solar cell is a prime contender for future terrestrial photovoltaic applications due to its relatively high efficiency, ~9%, and projected low cost. However, a modified form of this cell, in which a ternary alloy $Zn_xCd_{1-x}S$ is substituted for CdS, has resulted in an even higher efficiency due primarily to an enhanced open circuit voltage V_{oc}.[1] Using a band model for the heterojunction in which the open circuit voltage is controlled by interface state recombination,[2] V_{oc} can be increased by reducing both the electron affinity mismatch and lattic mismatch at the heterojunction interface. Matching the electron affinities increases the barrier height for reverse current, and decreasing the lattice mismatch reduces the density of localized interface states. Increased open circuit voltages have in fact been reported for $Cu_2S/Zn_xCd_{1-x}S$ photocells[3–5] with V_{oc} as high as 0.78 V for chemiplated (an aqueous cation exchange process)[6] Cu_2S layers on polycrystalline $Zn_{0.55}Cd_{0.45}S$ films.[5] The theoretical maximum V_{oc} value for a Cu_2S/(Zn,Cd)S cell is about 0.8 eV. However, while V_{oc} is increased by substituting (Zn,Cd)S for CdS, the short circuit current density generally decreases resulting in an overall decrease in the cell conversion efficiency.

One mechanism that has been proposed for the reduced current in chemiplated Cu_2S/(Zn,Cd)S photocells is excess Zn at the Cu_2S/(Zn,Cd)S interface[7,8] resulting in an interfacial potential energy spike. Since the collection efficiency for electrons generated in the Cu_2S layer is determined in part by their mobility in the $Zn_xCd_{1-x}S$ substrate and by the electric field at the edge of the depletion layer which lies almost entirely in $Zn_xCd_{1-x}S$, the interfacial chemistry is crucial. In this paper, we present results which show that the interface between chemimplated Cu_2S films on both polycrystalline and single crystal (Zn,Cd)S substrates is compositionally graded over distances of the order of tens to hundreds of nanometers and contains excess Zn, with respect to the average bulk Zn/Cd ratio, in the form of both elemental Zn and the compound ZnS.

II. EXPERIMENTAL PROCEDURE

Atomic absorption spectroscopy (AAS) combined with controlled chemical etching and Auger electron spectroscopy (AES) profiling with ion beam etching were used to obtain composition versus depth analyses in Cu_2S/(Zn,Cd)S photocells. The (Zn,Cd)S substrates were either polycrystalline layers or single-crystal wafers. The *n*-type polycrystalline (Zn,Cd)S films were deposited by thermal evaporation onto zinc-plated copper foil substrates.[9] For ZnS mole fractions between 0.10 and 0.20, film resistivities ranged from 1 to 50 Ω cm. Further details concerning the (Zn,Cd)S film deposition are contained in Ref. 9. Undoped *n*-type bulk single-crystal CdS and (Zn,Cd)S substrates were purchased commercially.

The Cu_2S layers were grown on CdS and (Zn,Cd)S using the chemiplating technique developed by Shiozawa *et al.*[6] An aqueous ion exchange bath containing 6 g/*l* of CuCl and 2 g/*l* of NaCl with a pH of ~3 was maintained at 98 °C, the same conditions used to produce operating photovoltaic devices. The ideal overall exchange reaction during film growth is

$$Zn_xCd_{1-x}S + 2CuCl \rightarrow Cu_2S + (1-x)CdCl_2 + x\,ZnCl_2 .$$

The reaction products $CdCl_2$ and $ZnCl_2$ go into solution as solid Cu_2S is formed. Figure 1 is a schematic diagram of the overall process. The reaction rate depends on the tempera-

 0021-8979/83/020982-05$02.40

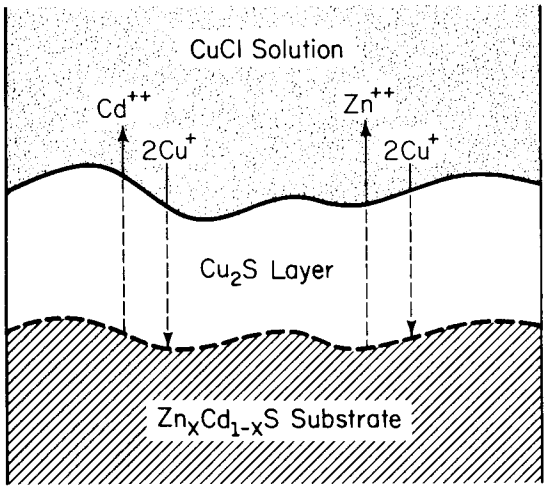

FIG. 1. Schematic representation of the chemiplating process used to form $Cu_2S/Zn_xCd_{1-x}S$ solar cells.

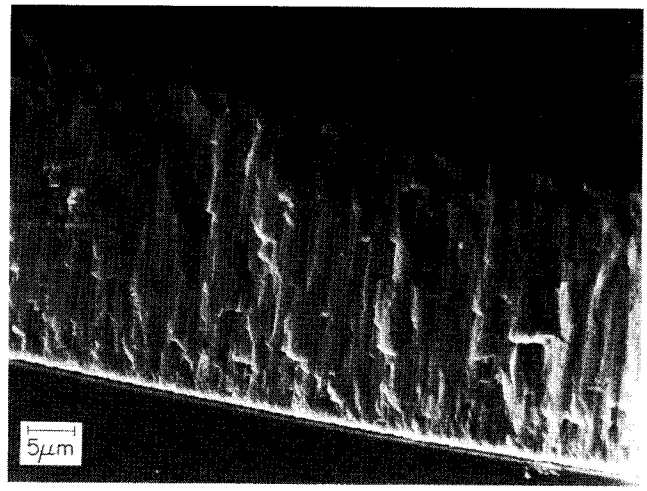

FIG. 2. Scanning electron micrograph showing the fracture cross section of an evaporated polycrystalline CdS layer.

ture, cuprous ion concentration in the solution, and grain structure and morphology of the $Zn_xCd_{1-x}S$ substrate or underlayer. In addition, differences between the solid solubility limits and the diffusion rates of Zn and Cd in Cu_2S may play a role, especially for thick films. In the present experiments, the initial film growth rate R was $\sim 2\ \mu$m/min on CdS, but R decreased with increasing Zn content on $Zn_xCd_{1-x}S$ substrates as observed previously.[4,9] Cu_2S growth was terminated by removing the sample from the plating bath and rinsing it in distilled water.

AAS measurements were carried out using a commercial flame spectrophotometer. For these analyses the samples were first etched in a 0.1 M KCN solution to remove Cu_2S and then in a 10:90 by volume $HCl:H_2O$ solution to remove $Zn_xCd_{1-x}S$. The concentrations of Cu, Zn, and Cd taken up in solution were then determined by atomic absorption at the following wavelengths: Cu (324.8 nm), Zn (213.9 nm), and Cd (228.2 nm). Quantitative results were obtained by comparison to standard solutions. Successive analyses using controlled etches provided composition versus depth information.

AES depth profiling was carried out in an ultra-high vacuum scanning Auger microprobe. Table I shows the Auger elemental peaks monitored. An Ar^+ ion beam operated at accelerating potentials between 0.4 and 1 keV was used for sputter etching. The primary electron beam current and accelerating potential were 1 μA and 5 keV, respectively, and the modulation voltage was 6 V.

TABLE I. Auger electron transitions monitored during compositional depth profiling of $Cu_2S/Zn_xCd_{1-x}S$ heterojunctions.

Element	Peak designation	Energy (eV)
C	*KLL*	272
Cd	*MNN*	376
Cl	*LMM*	181
Cu	*LMM*	920
O	*KLL*	510
S	*LMM*	152
Zn	*LMM*	994

III. EXPERIMENTAL RESULTS

The (Zn,Cd)S single-crystal substrates were prepared by cleaving and were thus oriented (0001). The polycrystalline CdS and (Zn,Cd)S underlayers were 30 μm thick, and scanning electron microscopy of the etched surface as well as of fracture cross sections showed that the films were columnar in structure with average grain sizes of 3 μm. Figure 2 shows a typical cross section from a CdS film. The (Zn,Cd)S layers were found to exhibit a strong (0002) preferred orientation as determined by x-ray diffraction (XRD). The copper sulfide overlayers were typically 0.5 to 1 μm thick, although layers $\sim 6\ \mu$m thick were grown. XRD and lattice constant analysis showed that all copper sulfide films, whether grown on single-crystal or polycrystalline substrates, were polycrystalline and primarily α-chalcocite in the orthorhombic structure. A partial Cu-S phase diagram, shown in Fig.3,[10] indicates that chalcocite is $Cu_{2-x}S$ where x is < 0.005. The average grain size of the Cu_2S films ranged from 2 to 4 μm with an (004) preferred orientation indicating a tendency for topotactic growth as the sulfur sublattice remained intact across the interface.

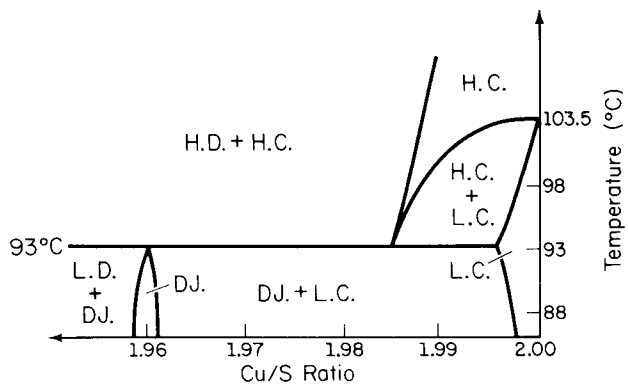

FIG. 3. Section of the Cu-S phase diagram.

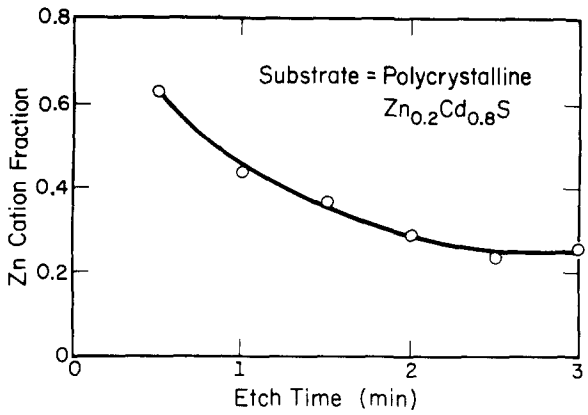

FIG. 4. Atomic absorption spectroscopy composition profile of polycrystalline $Zn_{0.2}Cd_{0.8}S$ alloy films onto which a $\sim$ 1-μm thick Cu_2S film was grown and chemically removed.

A series of experiments was carried out in which ~ 1 μm thick Cu_2S films were grown on polycrystalline $Zn_{0.2}Cd_{0.8}S$ underlayers and then removed by chemical etching in a 0.1 M KCN solution. AAS analysis indicated that the average Zn and Cd concentrations in the Cu_2S layers were <0.2 and 0.1 at. %, respectively. The $Zn_{0.2}Cd_{0.8}S$ underlayers were then themselves subjected to successive 1-min etches removing ~ 50 nm per etch in dilute HCl. Each etching solution was analyzed by AAS for Zn and Cd. The results, plotted in Fig. 4, show that a Zn-rich layer was formed at the heterojunction interface during the growth of Cu_2S. Furthermore, the amount of excess Zn was found to depend on the thickness of the Cu_2S overlayer. Figure 5 shows the Zn/Cd ratio measured after 1 min of etching from $Zn_{0.08}Cd_{0.92}S$ underlayers upon which had been grown Cu_2S films of different thickness. Although the data contains considerable scatter, it is clear that the amount of Zn accumulation at the heterojunction interface increased with the Cu_2S overlayer thickness.

AES analyses of Cu_2S/polycrystalline $Zn_xCd_{1-x}S$ heterojunctions agreed with the AAS results. Figure 6(a) shows a compositional depth profile of a $Zn_{0.2}Cd_{0.8}S$ film from

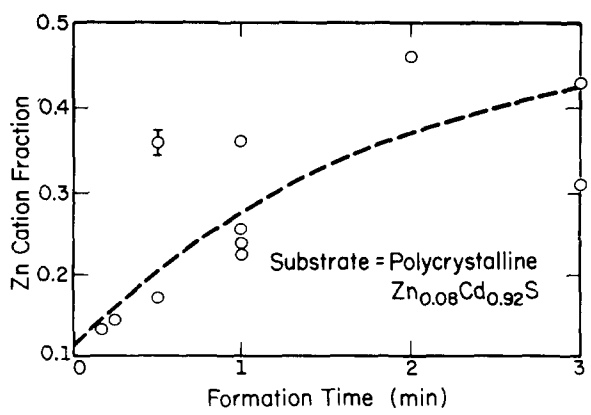

FIG. 5. Atomic absorption spectroscopy analysis of the upper ~ 500 Å of $Zn_{0.08}Cd_{0.92}S$ layers upon which successively thicker Cu_2S overlayers were grown and chemically removed. The results are plotted as a function of the formation time (i.e., film thickness) of Cu_2S.

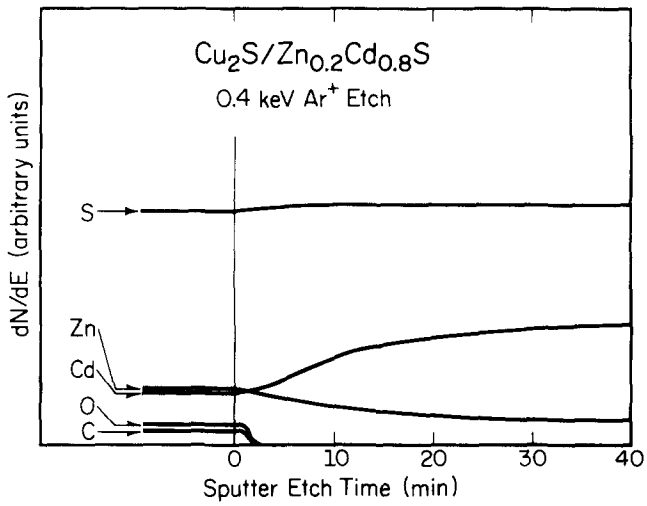

FIG. 6(a). Auger electron spectroscopy depth profile of a polycrystalline $Zn_{0.2}Cd_{0.8}S$ alloy film onto which a 0.8-μm thick Cu_2S layer was grown and chemically removed.

which a 0.8 μm thick Cu_2S layer had been chemically stripped. Sputter etching was carried out using a rastered 0.4-keV Ar^+ ion beam with a current density of 1.6×10^{14} ions cm^{-2} sec^{-1}. The diameter of the etched crater was 3 mm while the Auger signal was taken from a 100-μm diameter area near the central, approximately flat, region of the crater. The oxygen peak at the sample surface was due to air exposure. Figure 6(b) shows a depth profile, obtained under the same etching conditions, from an identical $Zn_{0.2}Cd_{0.8}S$ film which did not have a Cu_2S overlayer. A comparison of Figs. 6(a) and 6(b) again shows evidence for Zn accumulation at the heterojunction interface in agreement with the AAS results. This can be seen more clearly in Fig. 6(c).

Continuous AES profiles through both the Cu_2S and

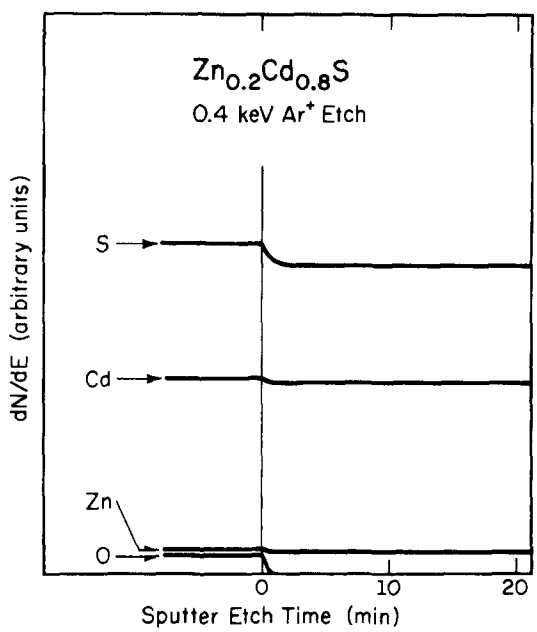

FIG. 6(b). Auger electron spectroscopy of a polycrystalline $Zn_{0.2}Cd_{0.8}S$ layer.

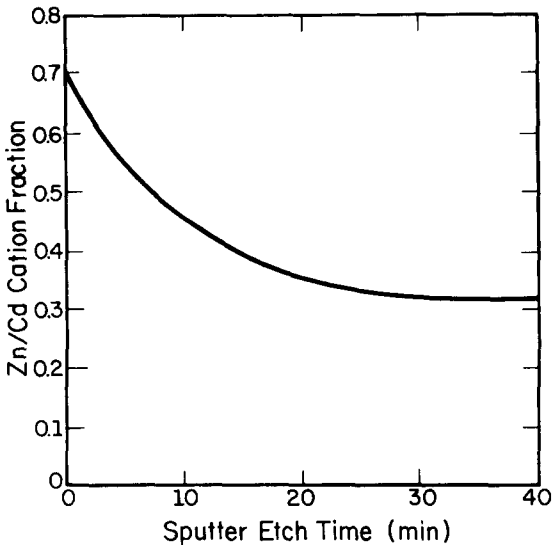

FIG. 6(c). Auger electron spectroscopy depth profile showing the Zn/Cd cation ratio in the $Zn_{0.2}Cd_{0.8}S$ sample corresponding to Fig. 6(a). Also see Fig. 4.

$Zn_xCd_{1-x}S$ layers were also obtained. In this case, single-crystal (Zn,Cd)S substrates were used to reduce both the broadening of the heterojunction due to incursion of Cu_2S down grain boundaries, and the anisotropy in Cu_2S formation rate that is characteristic of the rougher polycrystalline substrates. In all cases, regardless of the substrate Zn/Cd ratio, a compositionally graded junction at the $Cu_2S/Zn_xCd_{1-x}S$ interface was observed.

Figure 7(a) shows an Auger depth profile through a Cu_2S film on a single-crystal $Zn_{0.5}Cd_{0.5}S$ substrate. The film had a nominal thickness of 1.0 μm as determined from growth rate calibration curves using partially masked substrates. Sputter etching through the Cu_2S side of the interfacial region was carried out using a rastered Ar^+ ion beam with a current density J_i of 1.5×10^{14} ions cm^{-2} sec^{-1} at an acceleration energy E_i of 0.5 keV. J_i and E_i were increased to 1.9×10^{14} ions cm^{-2} sec^{-1} and 1.0 keV, respectively, near the (Zn,Cd)S side of the graded junction. Oxygen and carbon from air exposure and residual chlorine from the plating bath were observed at the sample surface. However, these signals decreased rapidly upon sputter etching and were no longer detectable after ~4 min of etching. Zn and Cd were also observed at the surface as well as throughout the bulk of all Cu_2S samples investigated, and the Zn/Cd ratio was always larger than that of the substrate. The Cu_2S/(Zn,Cd)S interfacial region extended over several tens to a few hundred nanometers, depending on film thickness, with very large excess Zn accumulations, as shown in Fig. 7(a). Figure 7(b) shows a Cu_2S/CdS depth profile for comparison. The width of the interfacial region was considerably narrower even though the actual Cu_2S film thickness was approximately the same as that shown in Fig. 7(a). In both cases, Cu penetrated deeply into the substrate indicating nonuniform film growth rates even across single-crystal substrate surfaces.

IV. DISCUSSION

Chemiplated Cu_2S/(Zn,Cd)S heterojunctions were compositionally graded over very wide regions with measurable Zn and Cd concentrations observed throughout the Cu_2S layers. In all cases, the film growth rate R on either polycrystalline CdS or (Zn,Cd)S substrates was found, for a given substrate composition, to be approximately constant with time. This indicates that for films with thicknesses on the order of a few micrometers or less, the overall kinetic rate limitation to Cu_2S growth by chemiplating was provided by the interface reaction rate rather than by cation diffusion through the growing film or ion transport through the solution. A diffusion rate limitation would have resulted in a parabolic relationship between film thickness and growth time rather than the linear relationship observed. In addition, the plating bath during film growth was saturated with cuprous ions at a density of $\sim10^{19}$ cm^{-3}, while the average growth rates only required $\sim10^{17}$ Cu^+ ions per sec per cm^2 of substrate, a rate which was easily supplied in the agitated

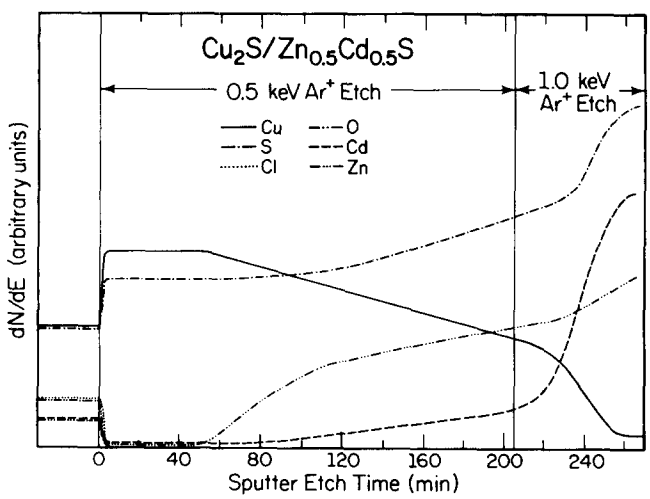

FIG. 7(a). Auger electron spectroscopy depth profile through a ~1-μm thick chemiplated Cu_2S film grown on a single-crystal $Zn_{0.5}Cd_{0.5}S$ substrate.

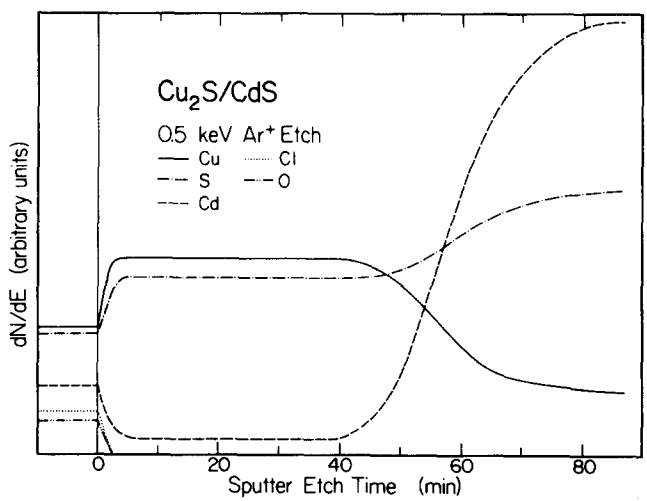

FIG. 7(b). Auger electron spectroscopy depth profile through a ~1-μm thick chemiplated Cu_2S film grown on a single-crystal CdS substrate.

solution.

Optical and scanning electron microscopy observations of as-deposited Cu_2S/(Zn,Cd)S cells showed distinct topographical features indicating nonuniform film growth rates R over the substrate surface area. In the case of polycrystalline substrates, this was due in part to differences in R with grain orientation. A similar effect occured with the cleaved single-crystal substrates due to multiple facet planes.[12] In addition, the diffusion rate of both reactants and products was more rapid down Cu_2S grain boundaries, giving rise to further lateral inhomogeneities.

AAS and AES depth profiling results from Cu_2S/(Zn,Cd)S cells demonstrated that Zn and Cd were distributed throughout the entire Cu_2S layer. Figure 7(a), typical of a series of AES profiles, shows that immediately below the bulk Cu_2S layer, the Cu concentration decreased rapidly as the Zn concentration increased with no corresponding increase in Cd. The S intensity remained essentially constant over this region. An analysis of elemental intensities compared to bulk standards indicated that zinc was present on the Cu_2S side of the graded junction as both elemental Zn and in the form of ZnS. Deeper into the interfacial region, the Cd signal began to increase with a correspondingly more rapid increase in S. The rate of change of all signals increased near the substrate end of the interface.

The above results can be explained by considering both reaction rates during the ion exchange process and the relative out-diffusion rates of Zn and Cd in Cu_2S. The exothermic free energies of formation of CdS and ZnS during the ion exchange process are 1.4 and 0.55 eV/molecule, respectively.[17] Thus the rate of the exchange reaction leading to the formation of $CdCl_2$ will be much faster than that of $ZnCl_2$, in agreement with observations that R decreased with increasing ZnS concentrations in the substrate, resulting in a net excess of ZnS in the interfacial region. The additional accumulation of metallic Zn near the bulk Cu_2S overlayer, which is consistent with the decreased short circuit currents in Cu_2S/(Zn,Cd)S cells, indicates that the Zn diffusion rate through Cu_2S is slower than that of Cd. The combination of excess Zn and ZnS in turn gave rise to the formation of much wider interfacial layers in these cells than in comparable Cu_2S/CdS solar cells.

Excess Zn and Cd remaining in the Cu_2S, and accumulation of Zn and ZnS near the Cu_2S/ZnCdS interface can adversely effect cell response by means of several mechanisms:

(1) On the Cu_2S surface, the metals appear mainly as oxides and sulfates, with Zn present primarily as ZnO.[13] Modifications of surface recombination velocities and surface electric fields caused by these species could reduce minority carrier collection.

(2) Excess Zn and ZnS near the junction would result in a potential energy spike in the heterojunction band structure and decrease the photogenerated current.[8,14]

(3) Unreacted metals in the Cu_2S (Zn in particular) would decrease conduction electron lifetimes and diffusion lengths.

(4) The electron mobility in $Zn_xCd_{1-x}S$ near the junction would be reduced,[15] thus increasing the fraction of photogenerated electrons lost to interface recombination.[16]

ACKNOWLEDGMENTS

The authors would like to acknowledge the use of the facilities in the Center for Micronanalysis of Materials, University of Illinois, which is partially supported by the DOE. In addition, the work of Uppal and Burton was supported by SERI through subcontract No. XS-0-9075-1, while Rivaud and Greene were supported by the DOE Division of Material Sciences under contract DE-AC02-76Er01198.

[1] R. B. Hall, R. W. Birkmire, J. E. Phillips, and J. D. Meakin, Appl. Phys. Lett. **38**, 925 (1981).
[2] A. Rothwarf and A. M. Barnett, IEEE Trans. Electron Devices **ED-24**, 381 (1977).
[3] L. C. Burton and T. L. Hench, Appl. Phys. Lett. **29**, 612 (1976).
[4] S. Martinuzzi, J. Oualid, D. Sarti, and J. Gervais, Thin Solid Films **51**, 211 (1978).
[5] V. P. Singh and J. F. Jordan, IEEE Electron Dev. Lett. **EDL-2**, 137 (1981).
[6] L. R. Shiozawa, R. Augustine, G. A. Sullivan, J. M. Smith, III, and W. R. Cook, Jr., Rep. ARL 69-0155 (Clevite Final Report), Clevite Corporation, Cleveland, Ohio (1969).
[7] L. C. Burton, Appl. Phys. Lett. **35**, 780 (1979).
[8] W. B. Hsu and L. C. Burton, J. Electron. Mater. **10**, 703 (1981).
[9] L. C. Burton, B. Baron, T. L. Hench, and J. D. Meakin, J. Electron. Mater. **7**, 159 (1978).
[10] R. Hill, *Active and Passive Thin-Film Devices*, edited by J. T. Coutts (Academic, New York, 1978), Chap. 10.
[11] A. E. Aerschodt, J. J. Capart, K. H. David, M. Fabbricotti, K. H. Heffels, J. J. Loferski, and K. K. Reinhartz, IEEE Trans. Electron Devices **ED-18**, 4771 (1971).
[12] P. F. Lindquist and R. H. Bube, J. Electrochem. Soc. **119**, 936 (1972).
[13] P. N. Uppal, D. W. Dwight, and L. C. Burton (in press).
[14] L. C. Burton, P. N. Uppal, and D. W. Dwight, J. Appl. Phys. **53**, 1538 (1982).
[15] S. Durand, Thin Solid Films **44**, 43 (1977).
[16] A. Rothwarf, Solar Cells **2**, 115 (1980).
[17] Progress Report XR-9-8063-1, Institute of Energy Conversion, University of Delaware, 1979, p. 17.